Electronic Supplementary Material (ESI) for Nanoscale.

Efficient Interlayer Confined Nitrate Reduction Reaction and Oxygen Generation Enabled by Interlayer Expansion

Ye Zhang,[a,†] Mengqiu Xu,[a,†] Xudong Xu,[a] Xiaoyu Li,[a] Genping Zhu,*[a] Gan Jia,[a] Bingchuan Yang,*[b,c] Ruilian Yin,[d] Peng Gao,[a] and Wei Ye*[a]

[a] College of Material, Chemistry and Chemical Engineering, Key Laboratory of Organosilicon Chemistry and Material Technology, Ministry of Education, Hangzhou Normal University, Hangzhou, Zhejiang 311121, China.
E-mail: yewei@hznu.edu.cn; zhugenping@hznu.edu.cn

[b] School of Chemistry and Chemical Engineering, Liaocheng University, Liaocheng 252000, Shandong, China.
E-mail: yangbingchuan@lcu.edu.cn

[c] School of Chemistry and Chemical Engineering, Shandong University, Jinan, 250100, China.

[d] College of Chemical Engineering, Zhejiang University of Technology, Hangzhou, Zhejiang 310014, China.

[†]These authors contribute equally.

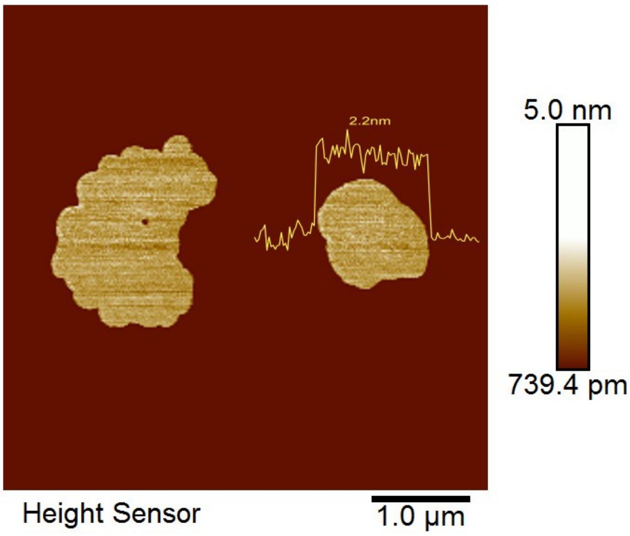

Fig. S1 AFM image of single α-$Ni_{0.881}Fe_{0.119}(OH)_2$ nanosheet.

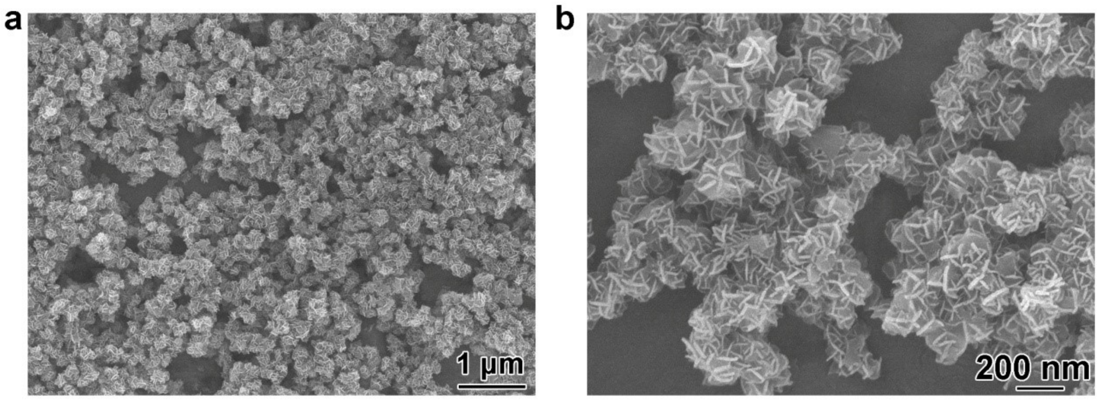

Fig. S2 (a,b) SEM images of α-$Ni_{0.881}Fe_{0.119}(OH)_2$ nanosheets.

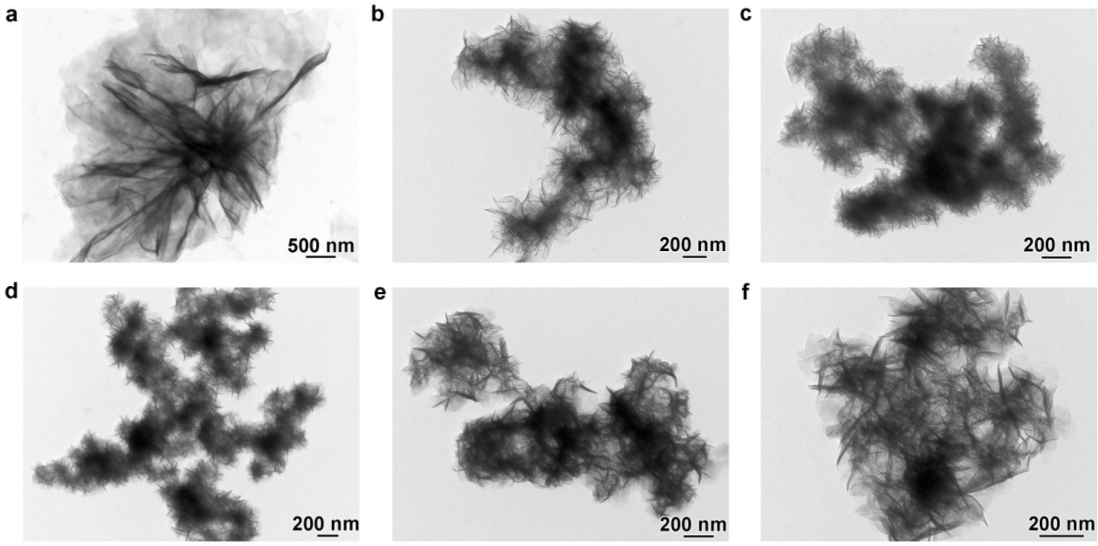

Fig. S3 TEM images of α-$Ni_{1-x}Fe_x(OH)_2$ nanosheets with different Fe doping levels: (a) x=0, (b) x=0.053, (c) x=0.098, (d) x=0.119, (e) x=0.150, (f) x=0.171.

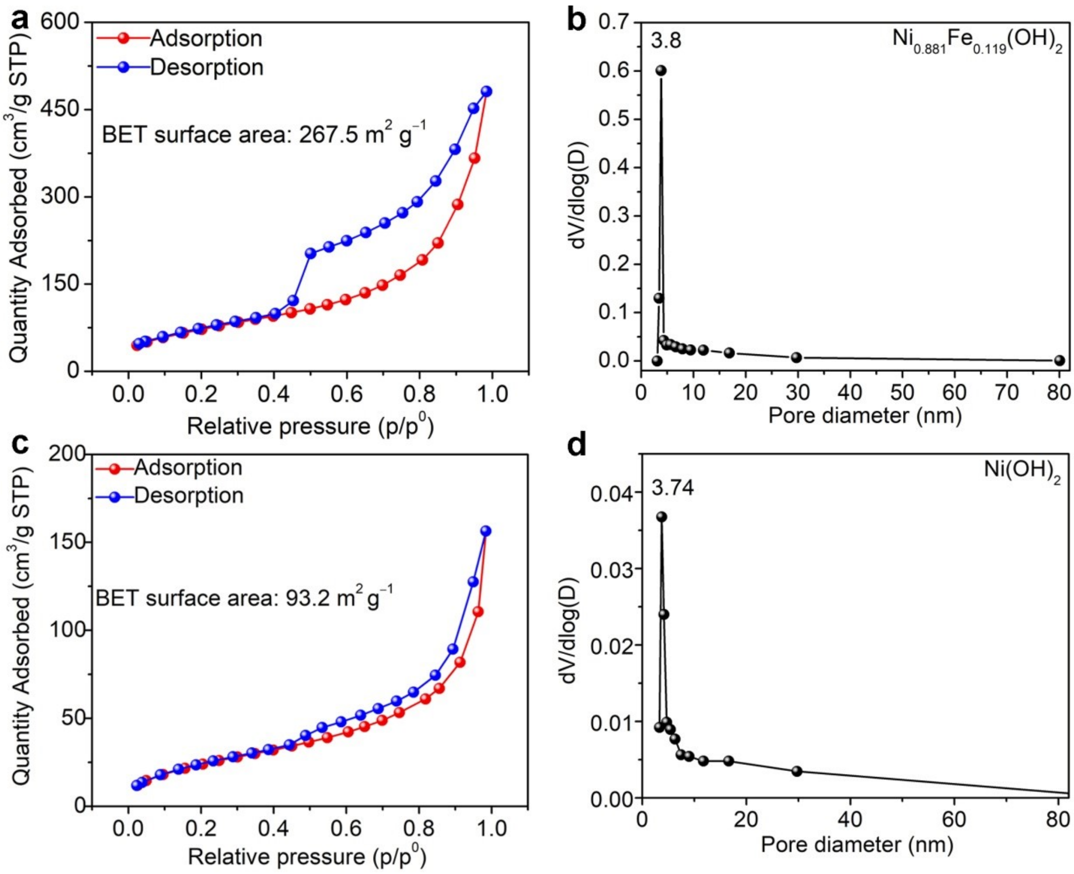

Fig. S4 Nitrogen adsorption-desorption curves and pore size distributions curves of (a,b) α-$Ni_{0.881}Fe_{0.119}(OH)_2$ nanosheets and (c,d) α-$Ni(OH)_2$ nanosheets.

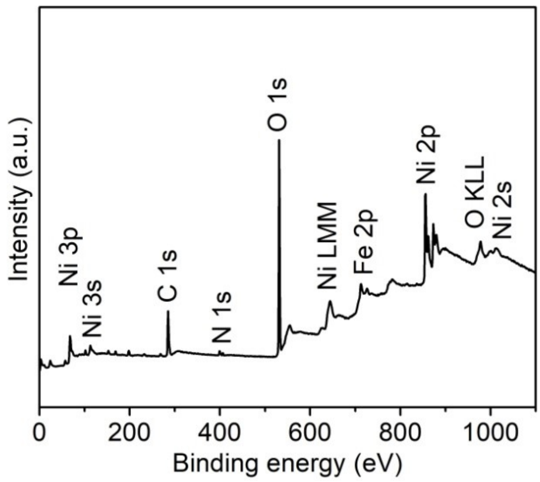

Fig. S5 XPS survey of α-$Ni_{0.881}Fe_{0.119}(OH)_2$ sample.

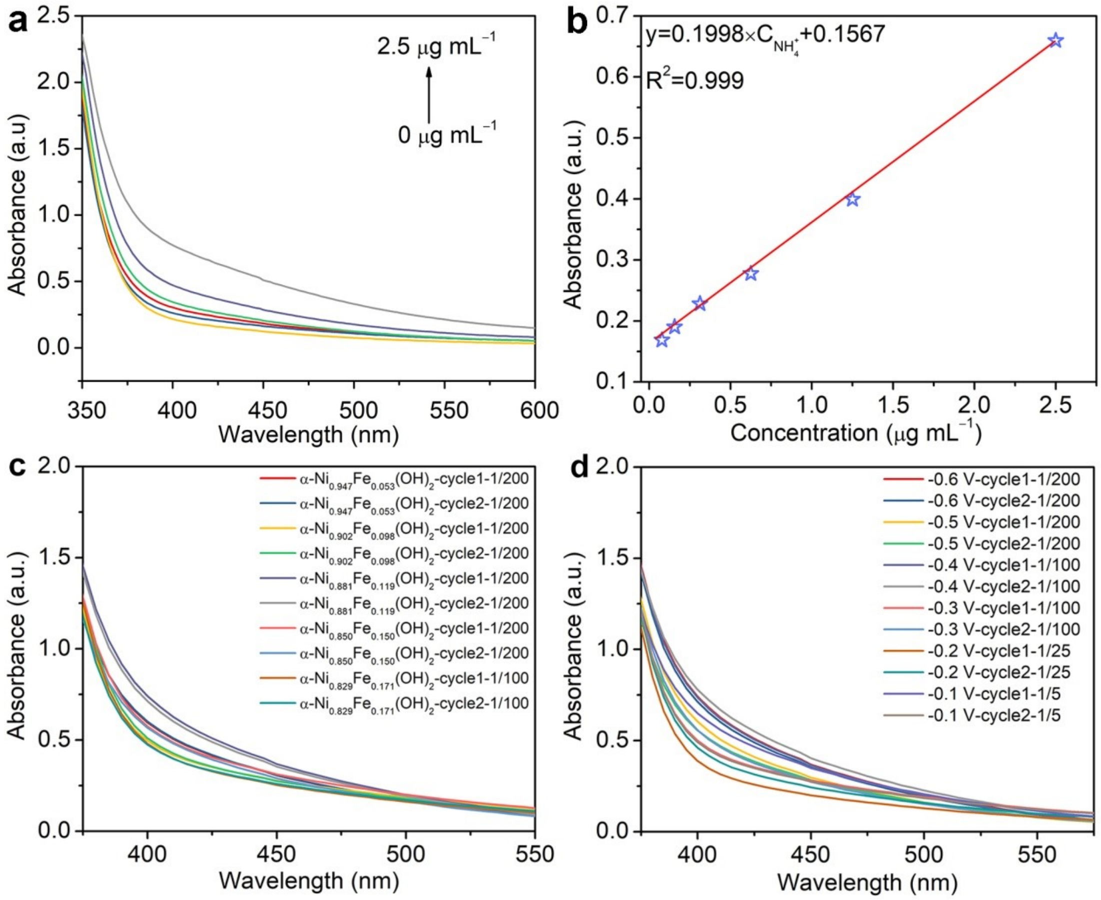

Fig. S6 (a) UV-vis absorption spectra based on spectrophotometry of Nessler's reagent and (b) NH_3 concentration-absorbance curve at 420 nm of standard NH_3 solutions with a series of concentrations. (c) UV-vis absorption spectra for α-$Ni_{1-x}Fe_x(OH)_2$ samples acquired at –0.6 V. (d) UV-vis absorption spectra for α-$Ni_{0.881}Fe_{0.119}(OH)_2$ nanosheets acquired at –0.6 to –0.1 V.

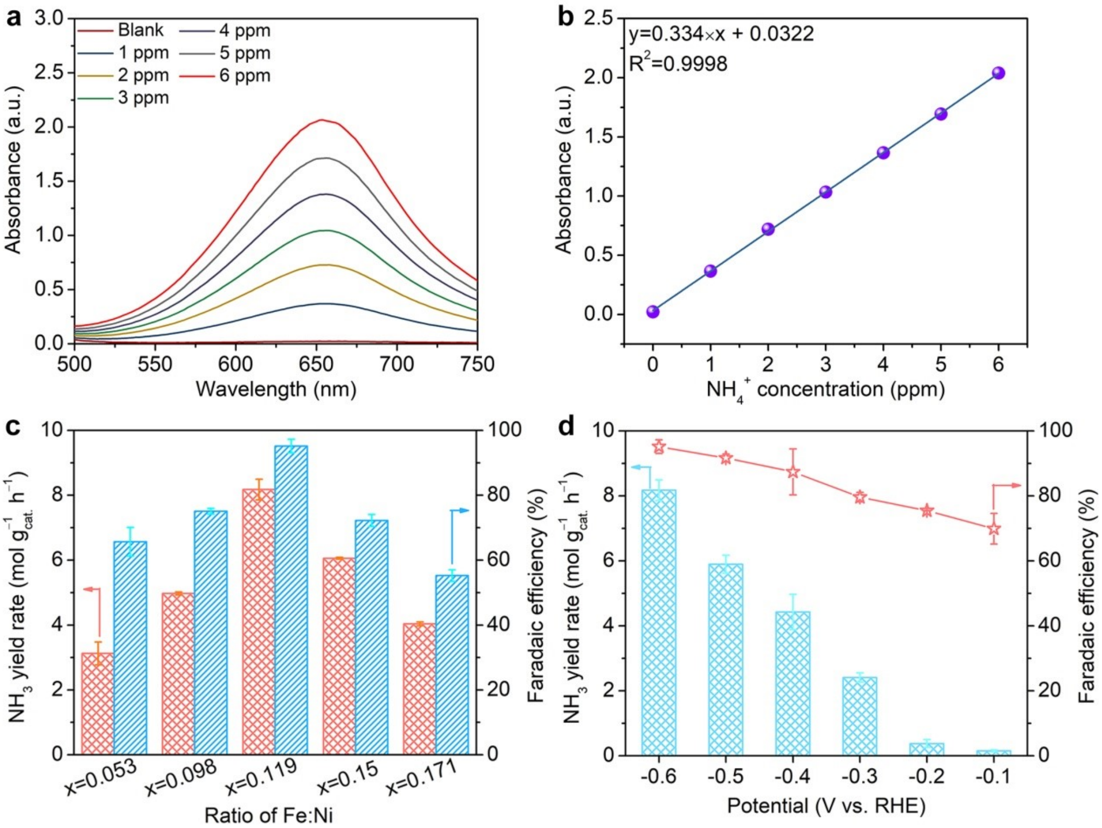

Fig. S7 (a) UV-vis absorption spectra based on spectrophotometry of indophenol blue method and (b) NH_3 concentration-absorbance curve at 655 nm of standard NH_3 solutions with a series of concentrations. (c) NH_3 yield rates and NO_3^--to-NH_3 FEs of α-$Ni_{1-x}Fe_x(OH)_2$ nanosheets at −0.6 V. (d) Potential-dependent NH_3 yield rates and FEs of α-$Ni_{0.881}Fe_{0.119}(OH)_2$ nanosheets.

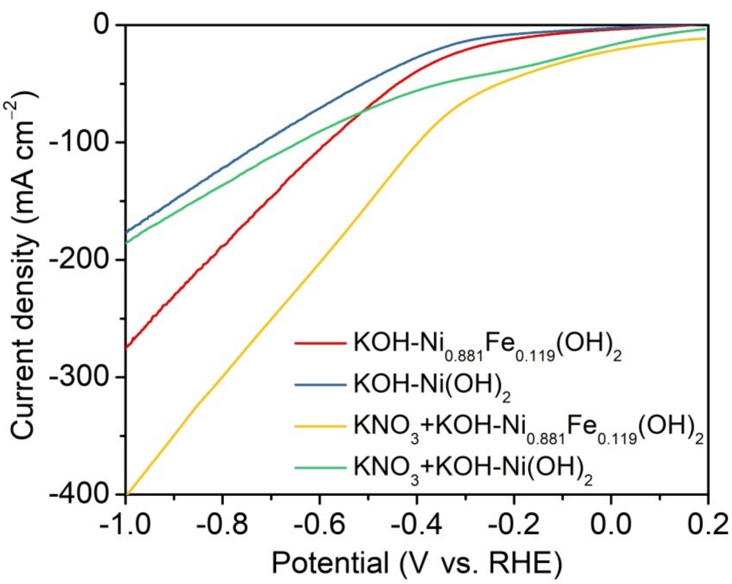

Fig. S8 The comparison of LSV curves for α-$Ni_{0.881}Fe_{0.119}(OH)_2$ and pristine α-$Ni(OH)_2$ nanosheets recorded in KOH or the mixture of KNO_3 + KOH.

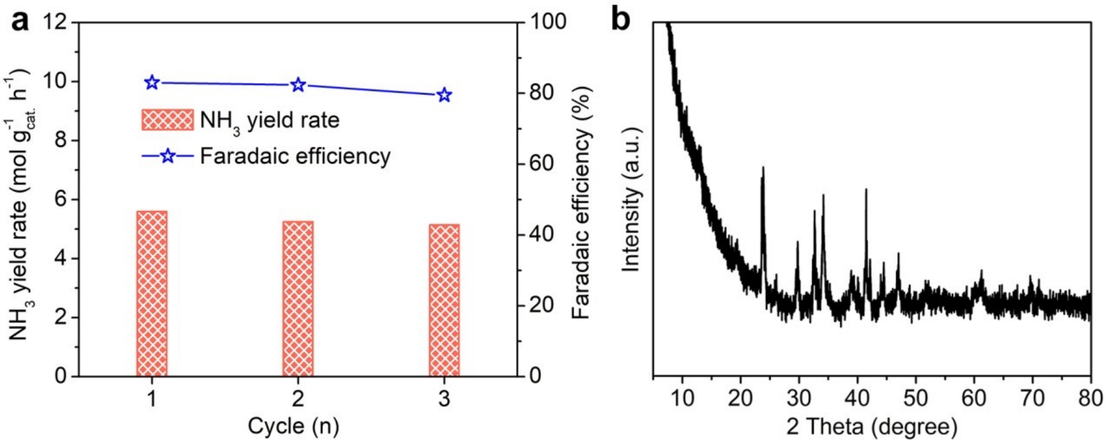

Fig. S9 (a) NH_3 yield rate and Faradaic efficiency for α-$Ni_{0.881}Fe_{0.119}(OH)_2$ sample recorded at –0.7 V. (b) XRD pattern of α-$Ni_{0.881}Fe_{0.119}(OH)_2$ after electrochemical catalysis at –0.7 V.

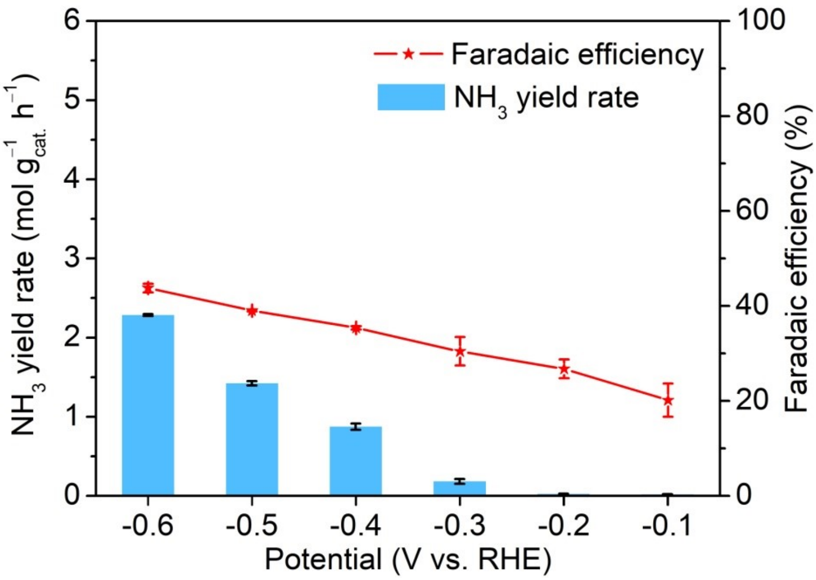

Fig. S10 Potential-dependent NH_3 production rates and FEs for α-$Ni(OH)_2$ nanosheets.

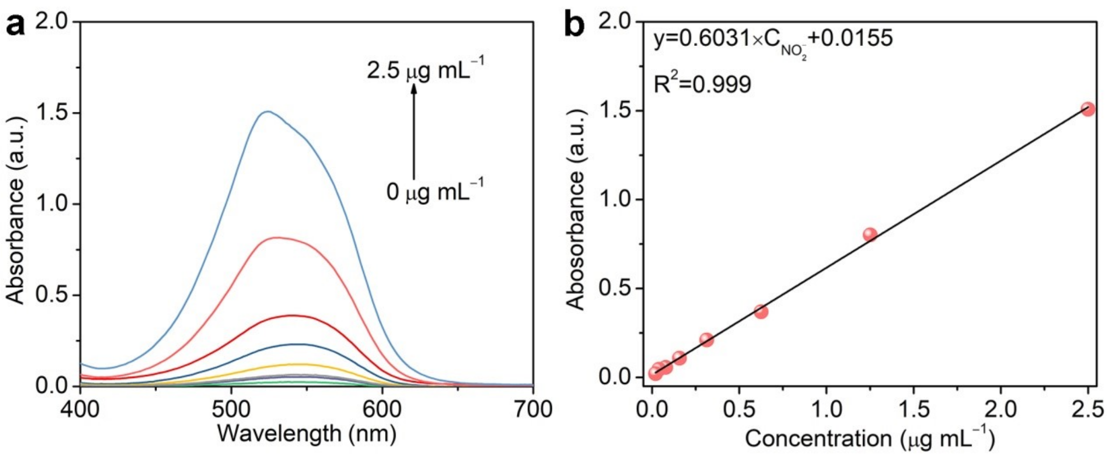

Fig. S11 (a) UV-vis absorption spectra and (b) concentration-absorbance curve of NO_2^- solutions with a series of standard concentrations.

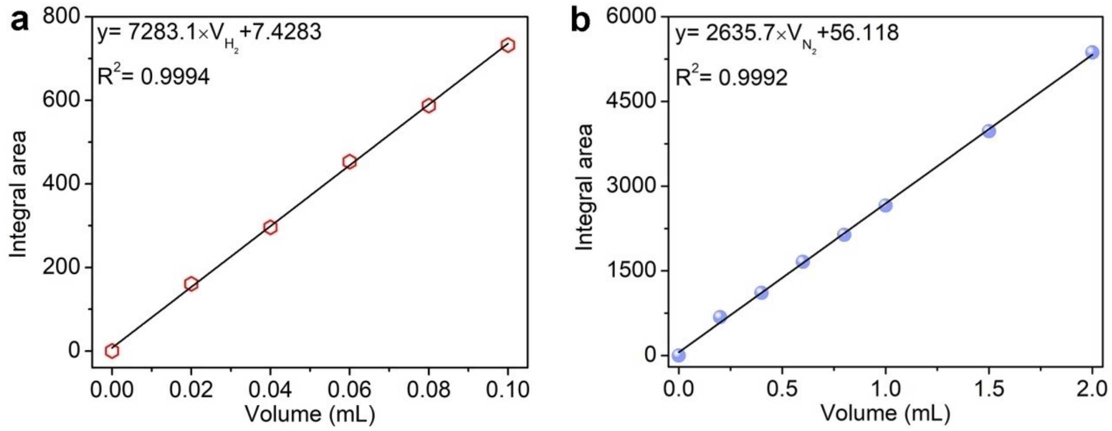

Fig. S12 Working curves for the determination of produced amount of (a) H_2 and (b) N_2.

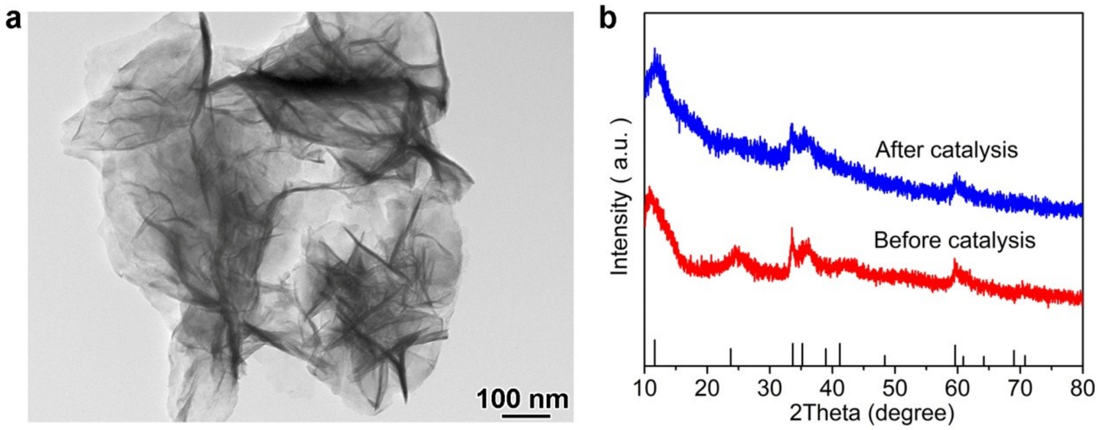

Fig. S13 (a) TEM image and (b) XRD pattern of α-$Ni_{0.881}Fe_{0.119}(OH)_2$ nanosheets after catalysis.

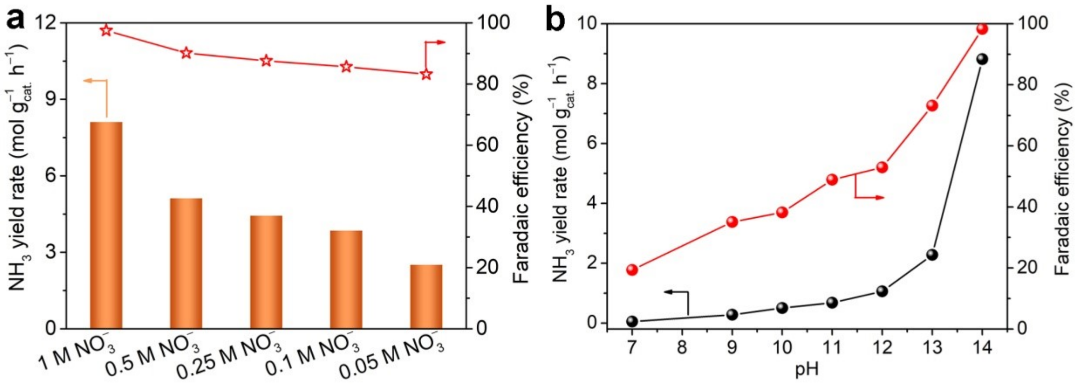

Fig. S14 (a) NH_3 yield rates and FEs of α-$Ni_{0.881}Fe_{0.119}(OH)_2$ nanosheets at (a) different concentrations of NO_3^- and (b) pH.

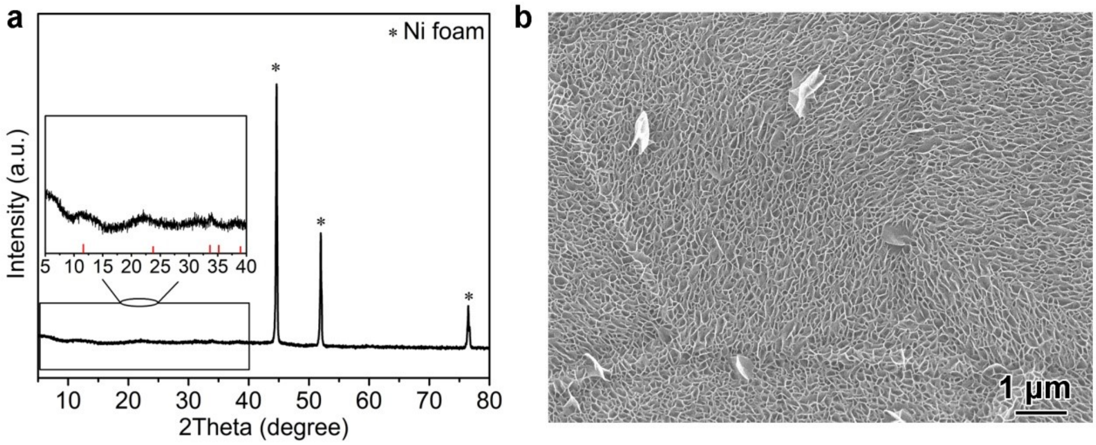

Fig. S15 (a) XRD pattern and (b) SEM image of α-$Ni_{0.881}Fe_{0.119}(OH)_2$ nanosheets arrays grown on nickel foam.

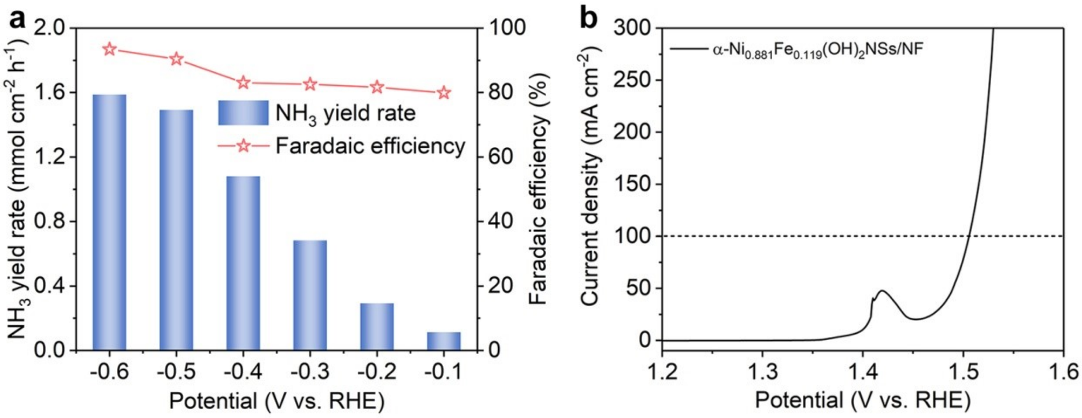

Fig. S16 (a) the NTRR and (b) OER performance of α-$Ni_{0.881}Fe_{0.119}(OH)_2$ nanosheet arrays on nickel foam.

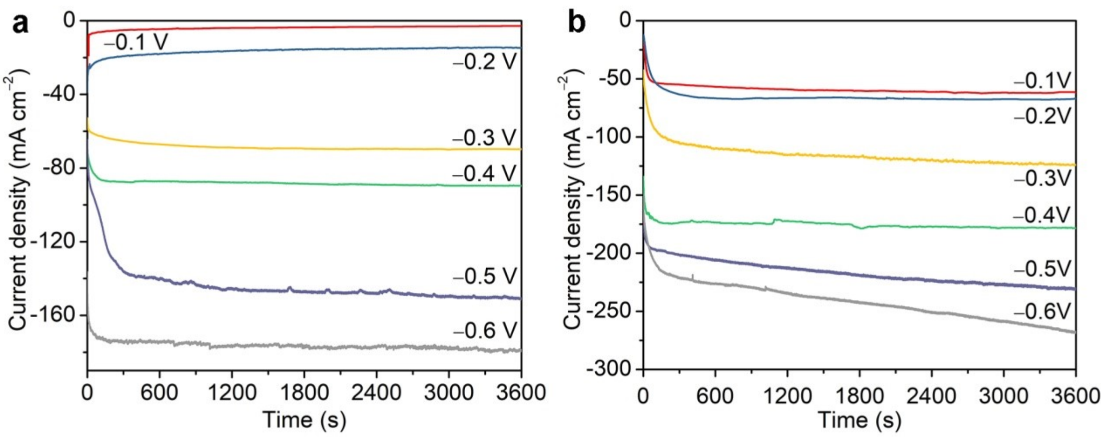

Fig. S17 *I-t* curves using α-$Ni_{0.881}Fe_{0.119}(OH)_2$ nanosheets as (a) cathodic catalyst and (b) bifunctional catalyst.

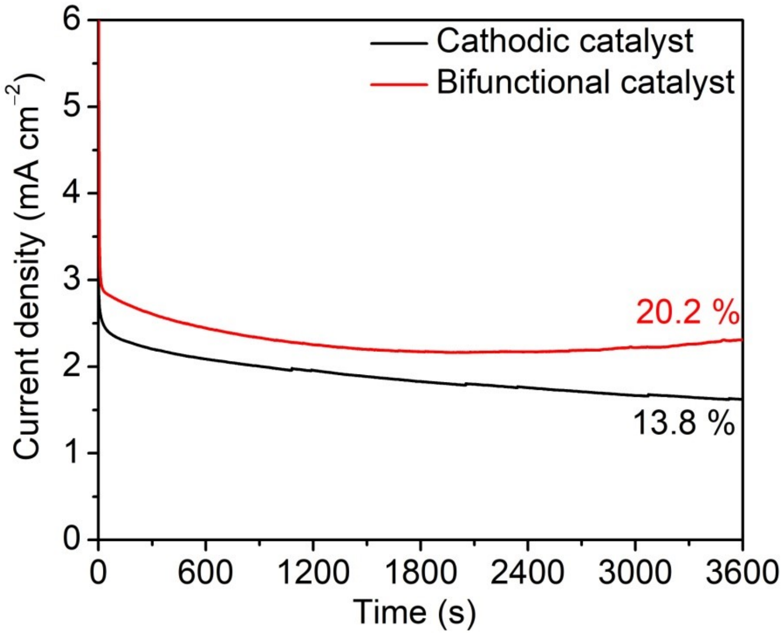

Fig. S18 *I-t* curves using α-$Ni_{0.881}Fe_{0.119}(OH)_2$ nanosheets as bifunctional catalyst or cathodic catalyst and the corresponding energy efficiencies.

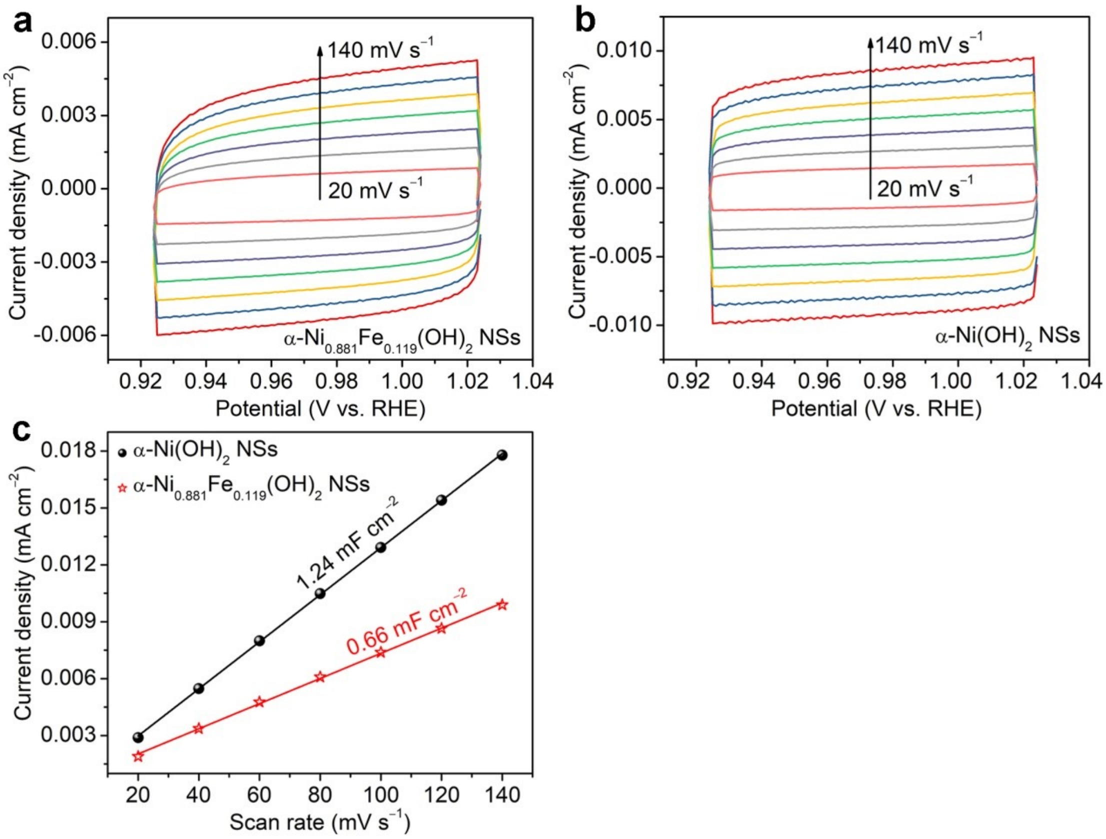

Fig. 19 Cyclic voltammetry curves recorded at different scan rates (20-140 mV s^{-1}): (a) α-$Ni_{0.881}Fe_{0.119}(OH)_2$ nanosheets, (b) pristine α-$Ni(OH)_2$ nanosheets. (c) Comparative C_{dl} for α-$Ni_{0.881}Fe_{0.119}(OH)_2$ nanosheets and α-$Ni(OH)_2$ nanosheets derived from CV curves with different scan rates.

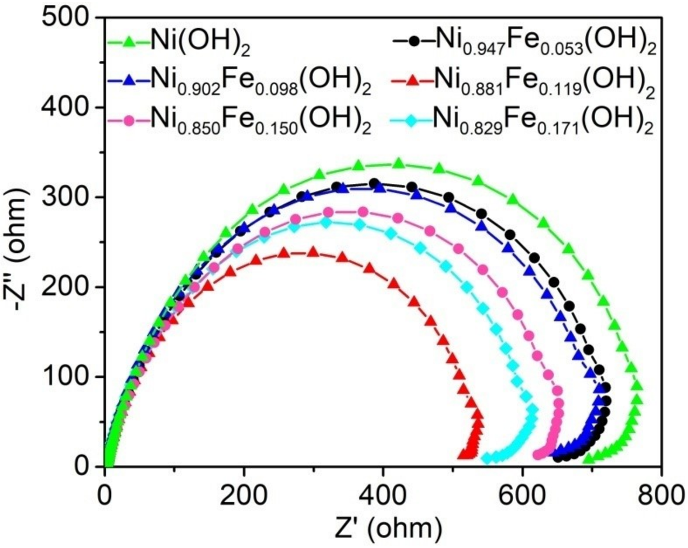

Fig. S20 EIS Nyquist plots for α-$Ni_{1-x}Fe_x(OH)_2$ nanosheets with different Fe doping levels (x=0, 0.053, 0.098, 0.119, 0.150, 0.171).

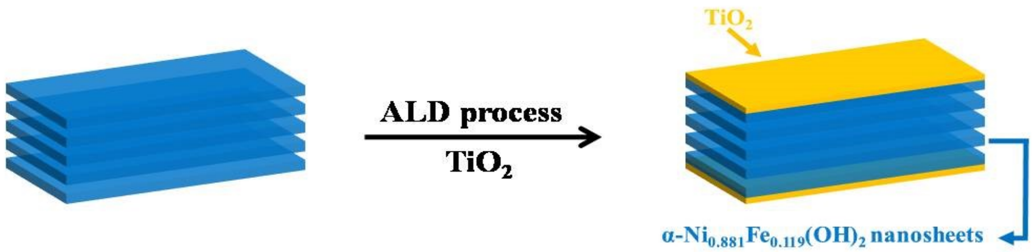

Fig. S21 Schematic illustration of atomic layer deposition to block the outmost layers of the layered α-$Ni_{0.881}Fe_{0.119}(OH)_2$ nanosheets.

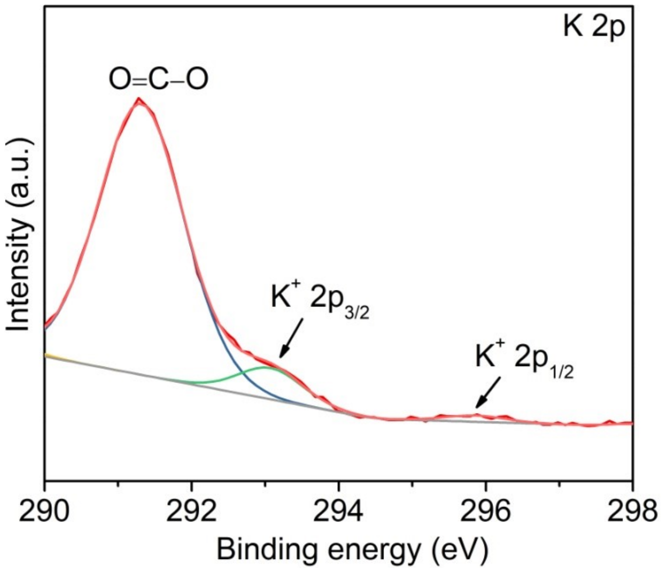

Fig. S22 K 2p spectrum of α-$Ni_{0.881}Fe_{0.119}(OH)_2$ samples after NTRR test.

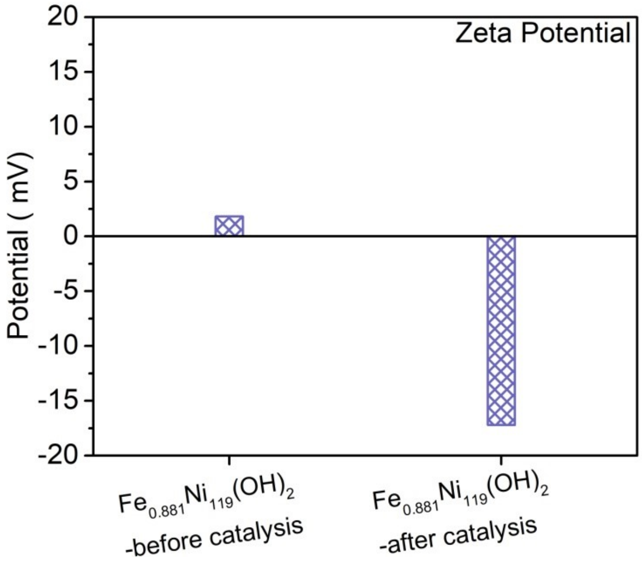

Fig S23. Zeta potentials of α-$Ni_{0.881}Fe_{0.119}(OH)_2$ nanosheets before or after catalysis.

Table S1. The mole ratios of Ni/Fe in the precursors and the corresponding x in the final α-$Ni_{1-x}Fe_x(OH)_2$ samples.

Ni/Fe ratios	x
1:0.1	0.053
1:0.2	0.098
1:0.3	0.119
1:0.4	0.150
1:0.5	0.171